Prediction of Monochrome Reflectance Spectra with an Extended Kubelka-Munk Model

Safer Mourad [*], *Patrick Emmel* [**], *Klaus Simon* [*], *and Roger David Hersch* [***]
[*]*Eidgenössische Materialprüfungs- und Forschungsanstalt (EMPA)*
[**]*Clariant–Masterbatches Division*
[***]*Ecole Polytechnique Fédérale de Lausanne (EPFL)*

Abstract

We present a prediction model for digital printers and more specifically for electrophotographic devices.

On the one hand, we propose an electrophotographic simulation model which estimates the microscopic structure of any printed toner layer based on its input halftone bitmap. Applying BOUGUER–BEER–LAMBERT's law, the obtained spatial toner arrangement yields the spectral transmittance distribution for non-light scattering colors. On the other hand, we introduce an extension to the KUBELKA-MUNK (KM) model, which allows to compute the halftone reflectance spectra from the estimated transmittance spectra. The extended KM model bridges the gap between the mathematical description of the optical point spread function of common office papers and the experimental results of simple reflectance measurements.

With the combination of the models, we are capable of predicting the reflectance spectra of a printed monochrome wedge with a mean estimation error of less than CIELAB $\Delta E^*_{94} = 1$.

1. Introduction

In electrophotography, it is hard to reproduce homogenous toner layers of uniform optical density values. Observed under a microscope, the printed dots appear mostly like clouds of randomly distributed toner particles. Occasionally, the particles are deposited beyond their target area and form extremely ragged dot edges. The high dot distortion causes a major difficulty in estimating the color of electrophotographic halftone patches and affects the tone reproduction curve to a high degree.

Another factor that affects halftone prints is the phenomenon of light scattering within common office papers. Some of the light that strikes an unprinted area around printed color particles, scatters within the substrate and emerges under the dithered toner film and vice versa. This creates a smoothing effect that is called the YULE–NIELSEN *effect* [1] or the *optical dot-gain* [2]. It causes the image to lose sharpness and to appear darker. With the decreasing dot size of modern high resolution printers, these combined effects become more and more significant.

To cope with both effects, we extend the KUBELKA–MUNK model in order to take into account the lateral light spreading responsible for the optical dot-gain. The model transforms a given point transmittance, $T_\lambda(x,y)$, i.e. the spectral transmittance factor at each point (x,y), to a point reflectance $R_\lambda(x,y)$. We then briefly present an electrophotographic simulation model which estimates the unknown point transmittance function $T_\lambda(x,y)$. Finally, we compare the prediction obtained by combining both models with measured spectra of monochrome halftone patches.

2. Light Scattering in Paper

Lateral light scattering is often modeled by a point spread function (*PSF*). In the literature, several approaches for modeling the point spread function of paper are known. Most of them were determined empirically, see for instance [1], or assume a specific type of function [3, 4]. Others are based on numerical simulations [2, 5], microscopic reflectance measurements [6], image processing [7], multiflux theory [8] or radiative diffusion [9].

Nevertheless, and due to its simplicity, the theory of KUBELKA–MUNK [10] has found a wide acceptance for modeling light scattering dull materials having the same surface characteristics over a wide area. The analysis is based on the simplified assumption of two diffuse light fluxes through the layer, one proceeding downward and the other simultaneously upward. This concept is not adapted to predict halftone prints on paper. This is due to the fact that halftone prints cannot be regarded as infinitely wide color layers and therefore laterally scattered rays cannot be neglected. In this respect, none of the early publications [11, 12, 13, a.o.] neither the bibliographical review given by [14] propose nor indicate how to deal with halftone prints.

However, BERG introduced isotropic light scattering

Proc. IS&T/SID, 10th Color Imaging Conference, Scottsdale (USA), 2002, Vol. 10, 298-304

within the framework of a KM oriented approach [15]. Still, his model remains restricted to two dimensions and disregards the influences of brighteners in paper or surface reflections. In the present article, we extend BERG's differential equation system to a cartesian three dimensional space. In this space, we establish a differential equation system taking into account absorption, scattering and paper fluorescence. By considering the reflections at the air coating boundaries, we specify the boundary conditions of the differential equation system. The final solution of the system is given by analytical equations in the FOURIER domain. They describe the reflectance and transmittance spectra as a function of different relevant optical constants, such as the FRESNEL reflections and transmittance factors and the specific scattering, absorptance and fluorescence coefficients.

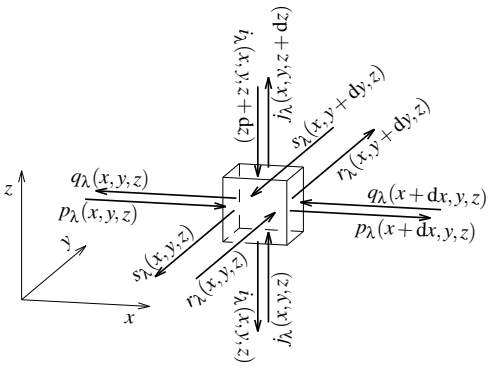

Figure 1: *Considered optical fluxes in a three dimensional paper section.*

2.1. Brightened Papers

Basically, the *point spread function* (PSF) of a brightened paper is affected by the included fluorescent additives. The supplied brighteners absorb a certain energy of the radiations within the invisible upper frequency band, called *the excitation spectrum* [16, 17]. A specific amount of that energy, defined by the *quantum yield*, is then released by radiative relaxation in the visible band, *the fluorescence spectrum*. This technique compensates for the yellowish appearance of natural non-brightened papers. But, as the emission of the fluorescence spectrum happens in all space directions within the paper's body, it acts like a diffuse partial light source or converter. By consequence, the brightening effect amplifies the point spread function of the paper in the bluish range of the visible light and must be taken into account when analyzing the PSF.

2.2. Spectral Three Dimensional Scattering Analysis

Lets λ be the wavelength of light and x,y,z be the spatial cartesian coordinates of a paper sheet of total thickness D (see Fig. 1). Considering a tiny cube of the paper sheet, we apply a wavelength dependent analysis of the up- and downward oriented light fluxes (i_λ, j_λ) as well as the lateral ones (p_λ, q_λ) and (r_λ, s_λ). For *isotropic* scattering, any light flux that enters the infinitesimal volume element $\mathrm{d}x\mathrm{d}y\mathrm{d}z$ from a specific direction loses a fractional amount $\sigma_\lambda \cdot \mathrm{d}x\mathrm{d}y\mathrm{d}z$ by scattering, $\alpha_\lambda \cdot \mathrm{d}x\mathrm{d}y\mathrm{d}z$ by absorption and $\phi_{a_\lambda} \cdot \mathrm{d}x\mathrm{d}y\mathrm{d}z$ by brightener excitation. At the same time, it gains a corresponding amount by scattering $\sigma_\lambda \cdot \mathrm{d}x\mathrm{d}y\mathrm{d}z$, from the other fluxes and by fluorescence $\phi_{f_\lambda} \cdot \mathrm{d}x\mathrm{d}y\mathrm{d}z$ from its own and from the other fluxes. Accordingly, a balance of radiant fluxes can be derived for each ray exiting the volume element, yielding for the particular case of i_λ

$$\begin{aligned} i_\lambda(x,y,z)\cdot\mathrm{d}x\,\mathrm{d}y = {} & i_\lambda(x,y,z+\mathrm{d}z)\cdot\mathrm{d}x\,\mathrm{d}y + \\ & \big[\,(\phi_{f_\lambda}-\phi_{a_\lambda}-\alpha_\lambda-5\cdot\sigma_\lambda)\cdot i_\lambda(x,y,z+\mathrm{d}z) + \\ & (\sigma_\lambda+\phi_{f_\lambda})\cdot\big(j_\lambda(x,y,z) + \\ & \quad p_\lambda(x+\mathrm{d}x,y,z) + q_\lambda(x,y,z) + \\ & \quad r_\lambda(x,y,z) + s_\lambda(x,y+\mathrm{d}y,z)\big)\,\big]\cdot\mathrm{d}x\,\mathrm{d}y\,\mathrm{d}z\,, \end{aligned} \tag{1}$$

with the spectral paper parameters:

α_λ, σ_λ specific absorption and scattering coefficients of the paper,

ϕ_{f_λ} normalized fluorescent spectrum, weighted by the quantum yield [16, Eq. (2)],

ϕ_{a_λ} specific fluorescent extinction coefficient of the brightening additives according to [16, Eq. (1)].

The radiance balances of the remaining fluxes (j_λ, p_λ, q_λ, r_λ and s_λ) are similar to Eq. (1) and can be derived according to Fig. 1.

The excitation spectrum of common brighteners is usually active only within the invisible light frequency band. Therefore, ϕ_{a_λ} is generally neglectable and set equal to 0 because the interest of the analysis is focused on the visible band of radiation only.

Analog to KM and BERG, we assume a linear variation of the fluxes along $\mathrm{d}x, \mathrm{d}y$, and $\mathrm{d}z$ which allows us to ignore higher order terms. Hence, forming from Eq. (1) a TAYLOR series expansion, we obtain a system of coupled linear partial differential equations

$$\begin{aligned} \frac{\partial i_\lambda}{\partial z} = {} & -(\phi_{f_\lambda}-\alpha_\lambda-5\cdot\sigma_\lambda)\cdot i_\lambda - \\ & (\sigma_\lambda+\phi_{f_\lambda})\cdot(j_\lambda+p_\lambda+q_\lambda+r_\lambda+s_\lambda)\,, \\ \frac{\partial j_\lambda}{\partial z} = {} & (\phi_{f_\lambda}-\alpha_\lambda-5\cdot\sigma_\lambda)\cdot j_\lambda + \\ & (\sigma_\lambda+\phi_{f_\lambda})\cdot(i_\lambda+p_\lambda+q_\lambda+r_\lambda+s_\lambda)\,, \end{aligned}$$

$$
\begin{aligned}
\frac{\partial p_\lambda}{\partial x} &= -\left(\phi_{f_\lambda}-\alpha_\lambda-5\cdot\sigma_\lambda\right)\cdot p_\lambda - \\
&\quad \left(\sigma_\lambda+\phi_{f_\lambda}\right)\cdot\left(q_\lambda+i_\lambda+j_\lambda+r_\lambda+s_\lambda\right), \\
\frac{\partial q_\lambda}{\partial x} &= \left(\phi_{f_\lambda}-\alpha_\lambda-5\cdot\sigma_\lambda\right)\cdot q_\lambda + \\
&\quad \left(\sigma_\lambda+\phi_{f_\lambda}\right)\cdot\left(p_\lambda+i_\lambda+j_\lambda+r_\lambda+s_\lambda\right), \\
\frac{\partial r_\lambda}{\partial y} &= \left(\phi_{f_\lambda}-\alpha_\lambda-5\cdot\sigma_\lambda\right)\cdot r_\lambda + \\
&\quad \left(\sigma_\lambda+\phi_{f_\lambda}\right)\cdot\left(s_\lambda+i_\lambda+j_\lambda+p_\lambda+q_\lambda\right), \\
\frac{\partial s_\lambda}{\partial y} &= -\left(\phi_{f_\lambda}-\alpha_\lambda-5\cdot\sigma_\lambda\right)\cdot s_\lambda + \\
&\quad \left(\sigma_\lambda+\phi_{f_\lambda}\right)\cdot\left(r_\lambda+i_\lambda+j_\lambda+p_\lambda+q_\lambda\right),
\end{aligned}
\tag{2}
$$

with neglected ϕ_{a_λ} and omitted coordinates dependencies (x,y,z) for improved readability.

2.3. Boundary Conditions

Choosing adequate boundary conditions is crucial. They strongly affect the accuracy and the complexity of the model. On the other hand, they build the connecting link between pure mathematics and observed physics. We assume non-fluorescent and weakly scattering inks.

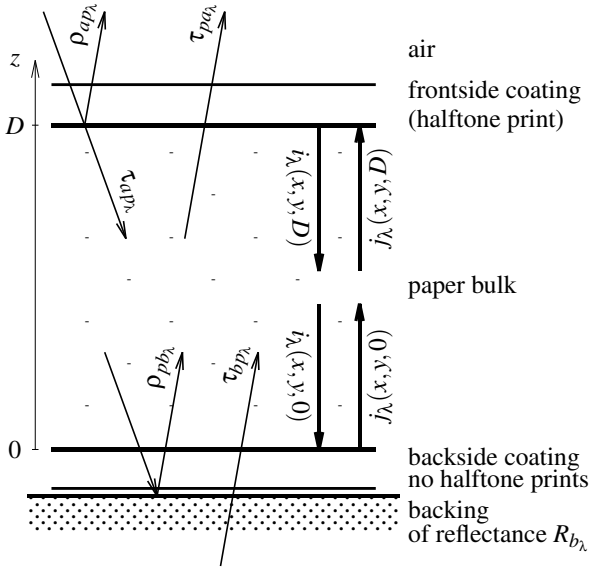

Figure 2: *Scheme of the considered boundary conditions.*

The paper is a translucent media and the optical conditions at the paper top and bottom boundaries have to be taken properly into account [18]. We assume a $(45/0^\circ)$ circularly illuminated printed paper sheet placed on a backing that has a spectral reflectance factor R_{b_λ}. While both paper faces could be covered with a coated or printed ink layer, only top-face *halftone* prints are allowed (see Fig. 2). Hereinafter, we use the word *coating* as a generic term which includes also any printed ink layer.

At the paper edges, any light flux that passes through the interfaces is subject to *multiple reflections* [19]. To consider the resulting density augmentation, we adopt the SAUNDERSON correction [20] which determines the fraction of light being transmitted or reflected by the interfaces. As the thickness of the layers is generally much thinner than the paper's body, we neglect any lateral spreading of the optical fluxes within the printed layers. In the case of a transmittance measurement, the fraction of light being transmitted through a transparent backing and the bottom coating layer is given by τ_{bp_λ}. Taking into account multiple reflections, τ_{bp_λ} is derived as the sum of the infinitive series of partially transmitted interreflections

$$
\begin{aligned}
\tau_{bp_\lambda} &= \tau_{s_\lambda}\cdot\mathcal{T}_{b_\lambda}+\tau_{s_\lambda}\cdot\mathcal{T}_{b_\lambda}\cdot\rho_{i_\lambda}\cdot\sigma_\lambda\cdot\mathcal{T}_{b_\lambda}^2+ \\
&\quad \tau_{s_\lambda}\cdot\mathcal{T}_{b_\lambda}\cdot\left(\rho_{i_\lambda}\cdot\sigma_\lambda\cdot\mathcal{T}_{b_\lambda}^2\right)^2+\cdots \\
&= \frac{\tau_{s_\lambda}\cdot\mathcal{T}_{b_\lambda}}{1-\rho_{i_\lambda}\cdot\sigma_\lambda\cdot\mathcal{T}_{b_\lambda}^2},
\end{aligned}
\tag{3}
$$

with the spectral parameters:

$\rho_{i_\lambda}, \tau_{i_\lambda}$ FRESNEL reflectance and transmittance factors at the inner side of the coating-air interface,

$\rho_{s_\lambda}, \tau_{s_\lambda}$ FRESNEL reflectance and transmittance factors at the outer side of the coating-air interfaces,

$\mathcal{T}_{b_\lambda}$ internal transmittance of the bottom-face coating (possibly a solid inked layer).

The scattering parameter σ_λ in the denominator of Eq. (3) is responsible for the multiple internal reflections at the back side coating.

In a similar manner, we approximate the spectral fraction of light which is reflected from the bottom coating and backing interface into the paper bulk by ρ_{pb_λ}

$$
\begin{aligned}
\rho_{pb_\lambda} &= \rho_{i_\lambda}\cdot\mathcal{T}_{b_\lambda}^2+\tau_{i_\lambda}\cdot R_{b_\lambda}\cdot\tau_{s_\lambda}\cdot\mathcal{T}_{b_\lambda}^2+\tau_{i_\lambda}\cdot R_{b_\lambda}^2\cdot\rho_{s_\lambda}\cdot\tau_{s_\lambda}\cdot\mathcal{T}_{b_\lambda}^2+ \\
&\quad \tau_{i_\lambda}\cdot R_{b_\lambda}^3\cdot\rho_{s_\lambda}^2\cdot\tau_{s_\lambda}\cdot\mathcal{T}_{b_\lambda}^2+\cdots \\
&= \mathcal{T}_{b_\lambda}^2\cdot\left[\rho_{i_\lambda}+\tau_{i_\lambda}\cdot\tau_{s_\lambda}\cdot R_{b_\lambda}\cdot\left(1+\rho_{s_\lambda}\cdot R_{b_\lambda}+\rho_{s_\lambda}^2\cdot R_{b_\lambda}^2+\cdots\right)\right] \\
&= (\rho_{i_\lambda}+\tau_{i_\lambda}\cdot\tau_{s_\lambda}\cdot\frac{R_{b_\lambda}}{1-\rho_{s_\lambda}\cdot R_{b_\lambda}})\cdot\mathcal{T}_{b_\lambda}^2.
\end{aligned}
\tag{4}
$$

The top surface transmits into the paper a fraction approximated by τ_{ap_λ} and a fraction out of the paper approximated by τ_{pa_λ}

$$
\tau_{ap_\lambda}(x,y) = \frac{\tau_{s_\lambda}(x,y)\cdot\mathcal{T}_{t_\lambda}(x,y)}{1-\rho_{i_\lambda}(x,y)\cdot\sigma_\lambda\cdot\mathcal{T}_{t_\lambda}(x,y)^2},
\tag{5}
$$

$$
\tau_{pa_\lambda}(x,y) = \tau_{i_\lambda}(x,y)\cdot\mathcal{T}_{t_\lambda}(x,y),
\tag{6}
$$

with the internal point transmittance $\mathcal{T}_{t_\lambda}$ at each point (x,y) of the front side coating (top halftoned surface). Additionally, a "specular" reflectance ρ_{ap_λ} must be taken into account at the front side. It represents the measured part of the light that reflects off the surface before entering the paper. ρ_{ap_λ} includes both pure FRESNEL reflectance and weakly scattered light within the top coating layer. According to our experience, best results are achieved by modeling the internal reflectance from the front side coating as follows

$$\rho_{ap_\lambda}(x,y) = \rho_s(x,y) \cdot \mathcal{T}_{t_\lambda}(x,y)^{p_{ink}}\,, \tag{7}$$

where p_{ink} is an exponent determined by the scattering power of the used ink.

Applying these corrections, the boundary conditions for the system of differential equations (2) in *reflectance* mode of a paper sheet of thickness D are

$$j_\lambda(x,y,0) = \rho_{pb_\lambda} ** i_\lambda(x,y,0)\,, \tag{8}$$
$$i_\lambda(x,y,D) = \tau_{ap_\lambda} \cdot i_{0_\lambda}\,, \tag{9}$$

where i_{0_λ} is the normalized illumination intensity in front of the coated paper. The two dimensional convolution in the (x,y) domain is indicated by $**$ needed due to the diffuse reflection at the backing of the light flux reaching the bottom side. Accordingly, for a paper illuminated by j_{0_λ} from the bottom side, the boundary conditions in *transmittance* mode are given by

$$j_\lambda(x,y,0) = \rho_{pb_\lambda} ** i_\lambda(x,y,0) + \tau_{bp_\lambda} \cdot j_{0_\lambda}\,, \tag{10}$$
$$i_\lambda(x,y,D) = 0\,. \tag{11}$$

Finally, before getting measured by a spectrophotometer, the upward light flux $j_\lambda(x,y,z)$ emerging from the scattering medium at D gets diffusely transmitted through the top coating layer $\tau_{pa_\lambda}(x,y)$. The normalized illuminating intensities i_{0_λ} and j_{0_λ} are set to 1 or 0 depending on the measuring setup, yielding the model of the measured reflectance and transmittance spectra

$$R_\lambda(x,y) = \rho_{ap_\lambda}(x,y) + \tau_{pa_\lambda}(x,y) ** j_\lambda(x,y,z)\,\big|_{z=D}\,. \tag{12}$$
$$T_\lambda(x,y) = \tau_{pa_\lambda}(x,y) ** j_\lambda(x,y,z)\,\big|_{z=D}\,. \tag{13}$$

2.4. Paper Modulation Transfer Function

The partial differential equation system Eq. (2) is of the same type as the one proposed in BERG's thesis and in the original KM work. The obtained system is simplified by applying the differentiation theorem of the two dimensional FOURIER transform [21] along the lateral dimensions x and y. Processing the obtained equation algebraically cancels four of the partial equations and the differentiations remains only in the perpendicular variable z. For the case of isotropic scattering we obtain the point reflectance spectrum

$$R_\lambda(x,y) = \rho_{ap_\lambda}(x,y) + \tau_{ap_\lambda}(x,y) \cdot \mathcal{F}_{x,y}^{-1}\Big[\mathcal{F}_{x,y}\big[\tau_{pa_\lambda}(x,y)\big] \cdot \frac{r_{1_{\xi\psi_\lambda}} + r_{2_{\xi\psi_\lambda}} \cdot \rho_{pb_\lambda} + e^{2Dc_{\xi\psi_\lambda}} \cdot (-r_{1_{\xi\psi_\lambda}} + r_{3_{\xi\psi_\lambda}} \cdot \rho_{pb_\lambda})}{d_{1_{\xi\psi_\lambda}} + d_{3_{\xi\psi_\lambda}} \cdot \rho_{pb_\lambda} + e^{2Dc_{\xi\psi_\lambda}} \cdot (d_{2_{\xi\psi_\lambda}} - d_{3_{\xi\psi_\lambda}} \cdot \rho_{pb_\lambda})}\Big]\,, \tag{14}$$

and the point transmittance spectrum

$$T_\lambda(x,y) = \tau_{bp_\lambda} \cdot \mathcal{F}_{x,y}^{-1}\Big[\mathcal{F}_{x,y}\big[\tau_{pa_\lambda}(x,y)\big] \cdot \frac{e^{Dc_{\xi\psi_\lambda}} \cdot t_{1_{\xi\psi_\lambda}}}{d_{1_{\xi\psi_\lambda}} + d_{3_{\xi\psi_\lambda}} \cdot \rho_{pb_\lambda} + e^{2Dc_{\xi\psi_\lambda}} \cdot (d_{2_{\xi\psi_\lambda}} - d_{3_{\xi\psi_\lambda}} \cdot \rho_{pb_\lambda})}\Big]\,, \tag{15}$$

with:

ξ, ψ the spatial frequencies,

$\mathcal{F}_{x,y}$ the FOURIER transform and $\mathcal{F}_{x,y}^{-1}$ its inverse.

The remaining coefficients $r_{1\cdots3_{\xi\psi_\lambda}}$, $t_{1_{\xi\psi_\lambda}}$ and $d_{1\cdots3_{\xi\psi_\lambda}}$ are dependent on the spatial frequencies and on the optical property coefficients given in Sec. 2.2. They are rather involved and prevent the inverse analytical FOURIER transformation of both expressions from being feasible. The remaining coefficients as well as a more detailed derivation will be presented in the Ph. D. of the first author, which will be published soon.

However, the obtained solution of the reflections and transmission spectra, are well suited for numerical transformation by an inverse two dimensional fast FOURIER Transform (FFT). Actually, the fractions in the second line of Eq. (14 and 15) describe the mathematically derived *Modulation Transfer Function* (MTF), i.e. the FOURIER transformed PSF of coated and brightened papers. With the extended SAUNDERSON correction terms ρ_{ap_λ}, ρ_{pb_λ}, τ_{ap_λ}, τ_{pa_λ} and τ_{bp_λ}, the solution accounts additionally for the multiple reflections occurring within the coatings at both sides of the paper for reflectance or transmittance considerations.

3. Computation of the Transmittance Spectra

The point transmittance distribution $\mathcal{T}_{t_\lambda}(x,y)$ is estimated applying BOUGUER–BEER–LAMBERT's law [22]. Assuming weakly light scattering inks, the mentioned law associates the internal transmittance $\vartheta_i(\lambda)$ of a filter i having the particular thickness δ_i to its normalized transmittance $\vartheta_{ref_i}(\lambda)$

$$\vartheta_i(\lambda) = \vartheta_{ref_i}^{\delta_i}(\lambda)\,. \tag{16}$$

Then, when printing M primary inks, the point transmittance distribution $\mathcal{T}_{t_\lambda}(x,y)$ is approximated by the product of the internal spectral transmittance distributions $\vartheta_{ref_i}(\lambda)$

$$\mathcal{T}_{t_\lambda}(x,y) = \prod_{i=1}^{M} \vartheta_{ref_i}^{\delta_i(x,y)}(\lambda)\,, \tag{17}$$

with an unknown ink relative thickness profile $\delta_i(x,y)$. How to estimate $\delta_i(x,y)$ is described in the following section.

4. Application for Electrophotographic Printers

For the case of common desktop laser printers, we calculate the point transmittance distribution $\mathcal{T}_{t_\lambda}(x,y)$ of Eq. (17) by applying an electrophotographic simulation model. The model is established on a microscopic grid with a resolution of $6.0\,\mu m$. The chosen resolution represents the lower average size of commonly used toners. In order to simulate the effects of each significant printer process step, a $2\times2\,mm$ wide color patch is simulated and passed from one sub-model to the other [23].

4.1. Electrostatic Field of Exposed Bitmaps

The surface of the photoconductive plate is assumed to be homogeneously charged during the charging step. Its surface charge is considered being neither dependent on the actual bitmap nor on the previously printed ones. In order to predict the deposited toner layers, the most significant process step is the constitution of the attracting electrostatic field formed by the exposed photoconductive plate according to the input bitmap. A suitable computation scheme is based on NEUGEBAUER's circular convolution kernel. In his publications [24, 25], he has shown that the density of an electrophotographic image is essentially given by the perpendicular component of the electrostatic field above the photoconductive plate. He introduced a Modulation Transfer Function $C(k)$ that relates the electrostatic field to the line exposure of a photoconductor

$$C(k) = \frac{A(k)}{B(k)} \cdot \cosh\big(k\cdot(L_1 - z)\big)\,, \tag{18}$$

with

$$A(k) = \sinh(k\cdot L_2) - \frac{\beta}{k\cdot L_2}\cdot\big(\cosh(k\cdot L_2) - e^{-\beta}\big)\,,$$

$$B(k) = \big[1-\big(\frac{\beta}{k\cdot L_2}\big)^2\big]\cdot\big[\cosh(k\cdot L_1)\cdot\sinh(k\cdot L_2) + \eta\cdot\sinh(k\cdot L_1)\cdot\cosh(k\cdot L_2)\big]\,,$$

and

- k exposed line frequency; line pairs per 2π microns,
- L_1 distance between the development electrode and the photoconductive plate,
- L_2 thickness of the photoconductive plate,
- β function of L_2, drift mobility, trapping time and the initial plate voltage,
- η dielectric constant of the plate,
- z average distance between the electrophotographic plate and the charges of the toner particles which will be developed.

The perpendicular electrostatic field component $E_{z_k}(u)$ of a single exposed line is determined by the inverse FOURIER transform $c(u)$ of the MTF given in Eq. (18) convolved with the intensity profile $I(u)$ of an exposure spot [26, Eq. (5.5)]

$$E_{z_k}(u) = I(u) * c(u)\,, \tag{19}$$

with

- u spatial line coordinate,
- c FOURIER-Transform of $C(k)$, evaluated numerically,
- I saturated GAUSSIAN intensity profile.

The circular convolution kernel $E_{z_k}(x,y)$ is approximated by rotating $E_{z_k}(u)$ around the vertical axis, basically implemented by substituting $\sqrt{x^2+y^2}$ for u. For any exposed bitmap, the overall perpendicular component of the attracting electrostatic field, which forms the latent image, is obtained by superposing the electrostatic field component $E_z(x,y)$ at each exposed printer dot (x,y).

4.2. Development, Transfer and Fusing

In the development nip [27], toner particles charged electrostatically are deposited according to the attracting electrostatic field $E_{z_k}(x,y)$ of the latent image. For simplicity, given the charges of the toners $q(x,y)$, it is assumed that the deposition of the particles occurs as soon as the attracting perpendicular component of the COULOMB force is strong enough to overcome the impeding adhesion force threshold th_{imp}

$$q(x,y)\cdot E_z(x,y) > th_{imp}\,. \tag{20}$$

Accordingly, the charge distribution influences the development behavior, and the size distribution mainly affects the micro transmittance structure of the printed result (Sec. 3). In order to model the toner charge and size distributions, the model utilizes a *lognormal* based probability density function describing the toner charges $q(x,y)$ and a RAYLEIGH based function describing the particles diameter $\delta_i(x,y)$ distributions [28].

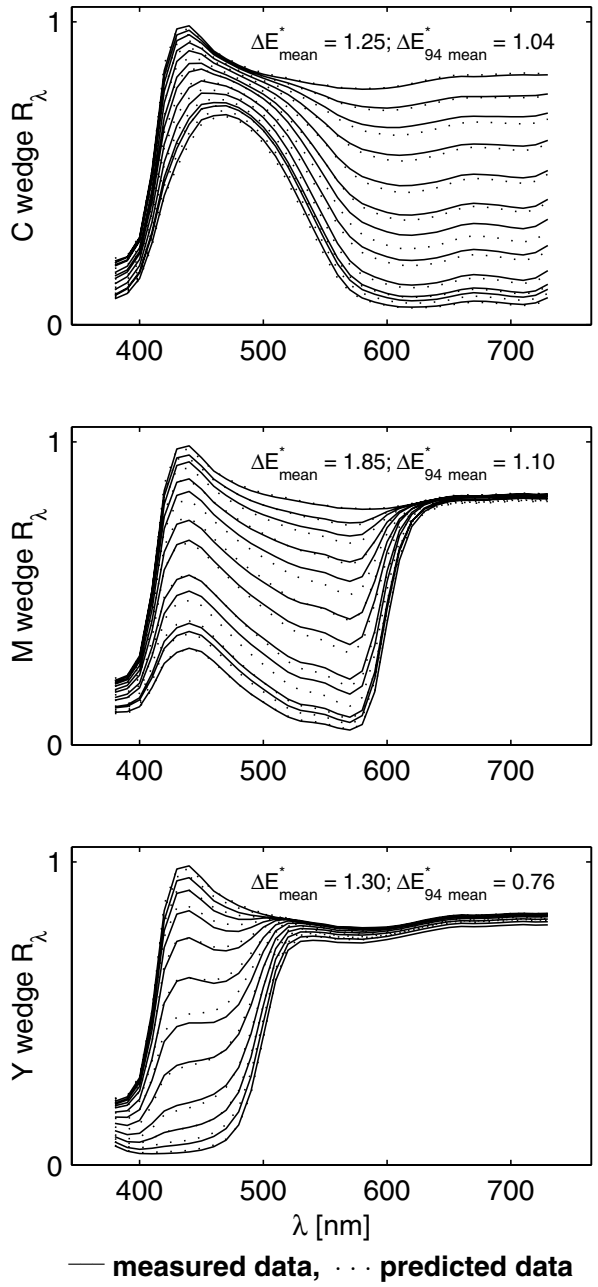

Figure 3: *Spectral* $(45/0^\circ)$ *reflectance predictions for the verification set of halftone wedges printed on a brightened high quality office paper.*

During the transfer process step, some of the developed toner particles may be rejected, resulting in an incomplete transfer efficiency. The lack of transfer is modeled by rejecting a proportional part of the developed toner particles.

Finally, after transferring the toner layers to a paper sheet, the image is fixed permanently by melting the toner to the medium. The main spreading effects within the fuser nip are simulated by applying a smoothing filter to the transferred particles. The applied filter convolution kernel is based on a hyper-parabola [28]. These filter operations yield the micro thickness profile $\delta_i(x,y)$ needed in Eq. (17) for each color layer i and each simulated high resolution grid pixel (x,y).

5. Experimental Results

The two independent models that we introduced, the light scattering as well as the electrophotographic model, incorporate many parameters which need to be estimated for each paper/printer combination. Generally, the calibration is performed by presenting a *calibration set* of measured spectra of different printed patches as an optimization goal to a constrained non-linear optimization routine of MATLAB™ [29].

The parameters of the light scattering model were estimated independently from the electrophotographic model. The calibration set consisted of measured spectra of the paper white and of printed solid patches of each considered primary color. After a completed optimization run, the light scattering parameters were fixed. Applying the light scattering model with the determined coefficients, the parameters of the electrophotographic model were estimated using measured spectral reflectance factors of 3 monochrome halftone prints of each considered primary color.

The estimation performance of the whole model is finally quantified by comparing the measured and predicted reflectance spectra of an extended extra set of 12 halftone patches (Fig. 3). The latest obtained colorimetric mean error is about CIELAB $\Delta E^* \approx 1.5$.

6. Conclusion

For the accurate prediction of the reflectance of halftone prints, we propose an extended model describing the interaction of light and halftone prints based on the concepts of KUBELKA-MUNK and the thesis of BERG. By taking the dominant optical scattering properties of common brightened office papers into account, it is possible to fit the model to measured spectral reflectances of printed solid patches. Thanks to our modified KM model and the extended SAUNDERSON corrections, we derived a mathematic description of the paper point spread function. In addition, we present a simulation model that approximates the microscopic point transmittance structure of electrophotographic halftone prints.

The monochrome mean prediction performance of the combined models reaches a color deviation error of less than CIELAB $\Delta E^* \approx 1.5$.

7. Biography

Safer Mourad received the M.S. degree in electrical engineering in 1993 from the Swiss Federal Institute of Technology (ETH), Zurich. From 1993 to 1997, he developed algorithms for real-time video tracking and high-end surveying instruments at Leica Geosystems. In 1998 he joined the Media Technology Department at the EMPA, St. Gallen and is currently working towards his Ph. D. His research interests include colorimetry, image processing and real-time control applications. He received the Swiss IEEE Award for his M.S. thesis and is a member of IS&T. E-mail address: safer.mourad@empa.ch

References

[1] F. R. Ruckdeschel and O. G. Hauser. Yule-Nielsen effect in printing: a physical analysis. *Applied Optics*, 17(21):3376–3383, November 1978.

[2] S. Gustavson. *Dot Gain in Colour Halftones*. PhD thesis, Dept. of Electrical Engineering, Linköping University, September 1997.

[3] G. Fischer, J. Rodriguez-Giles, and K. R. Scheuter. Ein physikalisches Modell für die Beschreibung von Lichtstreuprozessen. *Die Farbe*, 30(1/6):199–220, 1982.

[4] G. Rogers. Optical dot gain: Lateral scattering probabilities. In R. Eschbach, editor, *Recent Progress in Digital Halftoning II*, chapter V, pages 495–500. IS&T, 1999.

[5] L. Yang, S. Gooran, and B. Kruse. Simulation of optical dot gain in multichromatic tone reproduction. *Journal of Imaging Science and Technology*, 45(2):198–204, March/April 2001.

[6] I. Shinichi, Norimichi T., and M. Yoichi. Analyzing CTF of print by MTF of paper. *Journal of Imaging Science and Technology*, 42(6):572–576, November/December 1998.

[7] C. Neß and L. Göttsching. Übertragung von Linienrastern im Offsetdruck und deren drucktechnische Bedeutung. *Das Papier*, 47(7):353–363, 1993.

[8] J. J. Joshi, D. B. Vaidya, and H. S. Shah. Application of multi-flux theory based on Mie scattering to the problem of modeling the optical characteristics of colored pigmented paint films. *Color Research and Application*, 26(3):234–245, June 2001.

[9] G. Rogers. Optical dot gain in a halftone print. *Journal of Imaging Science and Technology*, 41(6):643–656, November/December 1997.

[10] P. Kubelka and F. Munk. Ein Beitrag zur Optik der Farbanstriche. *Zeits. f. techn. Physik*, (12):593–601, 1931.

[11] P. Kubelka. New contributions to the optics of intensely light-scattering materials. part I. *Journal of the Optical Society of America*, 38(5):448–457, May 1948.

[12] P. Kubelka. New contributions to the optics of intensely light-scattering materials. part II: Nonhomogenous layers. *Journal of the Optical Society of America*, 44(4):330–335, April 1954.

[13] J. K. Beasley, J. T. Atkins, and F. W. Jr. Billmeyer. Scattering and absorption of light in turbid media. In R.L. Rowell and Stein R.S., editors, *Electromagnetic scattering*, pages 765–785. 1967.

[14] B. Philips-Invernizzi and Dupont D. Bibliographical review for reflectance of diffusing media. *Optical Engineering*, 40(6):1082–1092, June 2001.

[15] F. Berg. *Isotrope Lichtstreuung in Papier - Neue Überlegungen zur Kubelka-Munk-Theorie*. PhD thesis, Technische Hochschule Darmstadt, April 1997.

[16] P. Emmel and R. D. Hersch. Spectral colour prediction model for a transparent fluorescent ink on paper. In *6th Color Imaging Conference*, pages 116–122. IS&T/SID, 1998.

[17] P. Emmel. *Modèles de prédiction couleur appliqués à l'impression jet d'encre*. PhD thesis, École Polytechnique Fédérale de Lausanne, `http://diwww.epfl.ch/w3lsp/publications/colour/`, 1998.

[18] S. Mourad, P. Emmel, K. Simon, and R. D. Hersch. Extending Kubelka-Munk's theory with lateral light scattering. In *International Conference on Digital Printing Technologies, NIP17*, pages 469–473, Fort Lauderdale, FL, 2001. IS&T.

[19] L. B. Tuckerman. On the intensity of the light reflected from or transmitted through a pile of plates. *Journal of the Optical Society of America*, 37(10):818–825, 1947.

[20] J. L. Saunderson. Calculation of the color of pigmented plastics. *Journal of the Optical Society of America*, 32(4):727–736, 1942.

[21] R. N. Bracewell. *The Fourier Transform and its Applications*. McGraw-Hill, 3rd. edition, 2000.

[22] G. Wyszecki and W. S. Stiles. *Color Science*. John Wiley & Sons, Inc., 2nd. edition, 1982.

[23] S. Mourad, P. Emmel, and R. D. Hersch. Predicting transmittance spectra of electrophotographic color prints. In *Color Imaging: Device-Independent Color, Color Hardcopy, and Graphic Arts VI*, volume 4300, pages 50–57, San Jose, CA, 2001. SPIE/IS&T.

[24] H. E. J. Neugebauer. A describing function for the modulation transfer of xerography. *Applied Optics*, 4(4):453–459, 1965.

[25] H. E. J. Neugebauer. Development method and modulation transfer function of xerography. *Applied Optics*, 6(5):943–945, 1967.

[26] E. M. Williams. *The Physics and Technology of Xerographic Processes*. John Wiley & Sons, Inc., 1984.

[27] L. B. Schein. *Electrophotography and Development Physics*. Laplacian Press, rev. 2nd. edition, 1996.

[28] S. Mourad, P. Emmel, and R. D. Hersch. Predicting monochrome color transmittance spectra of electrophotographic prints. In *International Conference on Digital Printing Technologies, NIP16*, pages 862–866, Vancouver, B.C., 2000. IS&T.

[29] MathWorks. MATLAB™ *Optimization Toolbox*, version 2.1.1, release 12.1, 2nd edition, 2001. consider especially lsqcurvefit and fmincon.